Impact of Random Alloy Fluctuations on inter-well transport in InGaN/GaN multi-quantum well systems: An atomistic non-equilibrium Green's function study

Michael O'Donovan[1,2]

E-mail: michael.odonovan@tyndall.ie

Mathieu Luisier[3]

E-mail: mluisier@iis.ee.ethz.ch

Eoin P. O'Reilly [1,2]

E-mail: eoin.oreilly@tyndall.ie

Stefan Schulz[1]

E-mail: stefan.schulz@tyndall.ie

[1]Tyndall National Institute, University College Cork, Cork, T12 R5CP, Ireland
[2]Department of Physics, University College Cork, Cork, T12 YN60, Ireland
[3]Integrated Systems Laboratory, ETH Zürich, 8092 Zürich, Switzerland

Abstract. Recent experimental studies indicate the presence of ballistic hole transport in InGaN multi quantum well structures. Widely used drift-diffusion models cannot give insight into this question, since quantum mechanical effects, such as tunneling, are not included in such semi-classical approaches. Also atomistic effects, e.g. carrier localization effects and built-in field variations due to (random) alloy fluctuations, are often neglected in ballistic transport calculations on InGaN quantum well systems. In this work we use atomistic tight-binding theory in conjunction with a non-equilibrium Green's function approach to study electron and hole ballistic transport in InGaN multi quantum well systems. Our results show that for electrons the alloy microstructure is of secondary importance for their ballistic transport properties, while for hole transport the situation is different. We observe for narrow barrier widths in an InGaN multi quantum well system that (random) alloy fluctuations give rise to extra hole transmission channels when compared to a virtual crystal description of the same system. We attribute this effect to the situation that in the random alloy case, $\mathbf{k}_{\|}$-vector conservation is broken/relaxed and therefore the ballistic hole transport is increased. However, for wider barrier width this effect is strongly reduced, which is consistent with recent experimental studies. Our findings

also provide a possible explanation for recent experimental results where alloying the barrier between the wells leads to enhanced ballistic (hole) transport in InGaN multi quantum well systems.

Keywords: NEGF, Transport, Nitride Submitted to: *J. Phys.: Condens. Matter*

1. Introduction

The semiconductor materials InN, GaN, AlN and their corresponding alloys have attracted strong interest for lighting applications due to their, in principle, flexible band gap engineering from the infrared to the ultraviolet part of the emission wavelength spectrum [1]. The alloy InGaN is of particular interest for light emitting diodes (LEDs) operating in the visible wavelength range. However, fundamental properties of these materials are not fully understood. For instance, InGaN-based LED structures undergo a so-called efficiency 'droop', which means that with increasing current density the internal quantum efficiency decreases [2–6].

Therefore, to analyze and guide the design of multi quantum well (MQW) InGaN-based LED structures with improved capabilities, their transport properties are often described in the framework of one-dimensional drift-diffusion models [7–9]. However, it has been highlighted that such an approach does not describe several key features of InGaN-based LEDs. This is reflected, for instance, in the finding that calculated I-V curves usually give much larger turn-on voltages when compared to experiment [10]. Studies have targeted this question by analyzing for instance ballistic carrier transport in InGaN multi quantum well (MQW) systems [11]. Here, one-dimensional calculations, assuming that InGaN is a homogenous alloy, that can be described by averaged parameters, have been performed. However, these studies did not predict any noticeable effect that would clarify the discrepancy between theory and experiment. Therefore, an often used approach is to reduce the intrinsic electrostatic built-in fields in the simulations by reducing the literature piezoelectric coefficients strongly (factor of order 2), in order to fit I-V curves to experimental data [12,13]. The underlying physical origin however is not clear for such a drastic assumption. Studies by Li *et al.* have shown that the alloy microstructure, namely random alloy fluctuations, significantly affect the I-V curves of a device [14]. Such approaches require three-dimensional (3-D) transport models to achieve an improved description of device characteristics. These 3-D calculations often build on modified continuum-based models for the electronic structure of the active region [15].

However, even though these models give an improved description of transport properties, other factors, such as ballistic electron or hole transport, are usually not well described by standard semi-classical transport models, since they do not account for quantum mechanical effects, such as tunneling. Recently developed localization landscape theory based models partly introduce quantum corrections in a drift-diffusion approach [14].

On the other hand, experimental studies observe significant ballistic hole transport through InGaN MQWs [16]. Understanding hole transport properties in these structures is important since ideally the carrier density (electrons and holes) should be evenly distributed in the wells forming the MQW; this ensures that all wells contribute to the light emission process. Low hole transport results in the situation that holes populate wells only close to the p-doped region of the device. Taking all this together,

the theoretical description of InGaN/GaN MQW systems asks therefore for a full 3-D model that captures both atomistic alloy induced effects as well as quantum mechanical contributions such as tunneling.

In this work we address this question in a fully 3-D atomistic and quantum mechanical frame. On the electronic structure side, an atomistic tight-binding (TB) model, which includes local strain and intrinsic built-in potential fluctuations due to random alloy fluctuations, is applied to capture carrier localization effects on a microscopic level. To achieve a quantum mechanical description of ballistic transport properties we employ the non-equilibrium Green's function (NEGF) approach, implemented in OMEN [17]. Using this framework we study transmission spectra of electrons and holes through InGaN MQW systems. To investigate the impact of alloy disorder, results are compared to the outcome of calculations that utilize a virtual crystal approximation (VCA) for the InGaN MQWs. Our data shows that for electron ballistic transport the alloy microstructure is of secondary importance for their ballistic transport properties, while for hole transport the situation is different. We observe that for narrow barrier width in an InGaN MQW system, the presence of the alloy fluctuations gives rise to extra hole transmission channels when compared to a virtual crystal description of the same system. We attribute this effect to the situation that in the random alloy case, $\mathbf{k}_{\parallel}$-vector conservation is broken/relaxed and therefore the ballistic hole transport is increased. Thus a VCA description would underestimate the contribution from hole ballistic transport properties in general. However, for wider barrier width this effect is strongly reduced. Overall, our theoretical findings of significant ballistic hole transport for narrower barrier width, which decreases as the barrier width is increased, is consistent with recent experimental studies [16].

Furthermore, the gained insight indicates also that alloying the barrier region between the wells with In (e.g. 5%) may be beneficial for carrier transport in InGaN MQW system. Such an approach results in (i) the breakdown of $\mathbf{k}_{\parallel}$-vector conservation and (ii) a slight reduction in the barrier height between the wells. As a consequence, especially the holes may be more evenly distributed between the different wells. Thus, ideally all wells may be contributing to the light emission process and improve therefore the efficiency of the corresponding device.

The paper is organized as follows. Section 2 gives a brief overview of the employed TB model and the NEGF framework. The details and features of the model MQW systems used in our study are outlined in Sec. 3. The results of our calculations are presented in Sec. 4. Finally, Section 5 summarizes the results of our work.

2. Theoretical Framework

To capture the effects of alloy fluctuations on a microscopic level, and its impact on ballistic transport properties, our electronic structure model is an atomistic nearest neighbor sp^3 TB model. The model is described in detail in Refs. [18] and [19] and we summarize briefly its main ingredients. To obtain the TB parameters of the binary

materials, the TB bandstructures are fitted to hybrid-functional density functional theory (DFT) data. To treat InGaN alloys we proceed as follows. The nearest-neighbour environment for cations (In,Ga) consists always of N atoms. However, N atoms can have variable numbers of In and Ga atoms as nearest neighbours. In the alloy, weighted averages of the InN and GaN binary values are used to determine the N onsite energies; this is a widely used approximation in the literature [20–22]. Given the large lattice mismatch between InN and GaN (approximately 10%), it is important to describe (local) strain effects in InGaN/GaN MQWs. To this end we apply a valence-force field model to calculate the relaxed atomic positions in such a system [18]. In what follows, our attention is directed towards *c*-plane InGaN/GaN MQWs. These systems exhibit very large electrostatic built-in fields, which are taken into account by the local polarization theory model described and discussed in Ref. [19]. An LED structure exhibits also an electrostatic built-in field due to *n*- and *p*-doped regions of the device. This field modifies conduction (CBE) and valence band edge (VBE) of the MQWs further. Therefore, to simulate and analyze transport properties of an LED-relevant active region using InGaN MQW systems the potential profile from a $p-i-n$ junction is calculated with NextNano [23] using a mesh size of 0.1 nm. The potential profile is calculated in 1-D using GaN material parameters from [24] and dielectric constants from [25]. InGaN QWs are not included at this step of the calculation. Instead, the potential profile from the $p-i-n$ junction is mapped onto the TB mesh, and included as a correction to the QW region in addition to the built-in field from local polarization theory. To calculate transport properties in an atomistic and quantum mechanical framework, we use the TB model as the starting point for NEGF based calculations. More specifically, the TB Hamiltonian is connected to the NEGF solver OMEN. OMEN takes input of the TB Hamiltonian, and modifies it to include for open boundary conditions. As electron-phonon scattering is not considered in ballistic transport, the transport is computed using the wavefunction formalism (or Quantum Transmitting Boundary Method) [17], as implemented in OMEN.

Overall, the aim of this study is to gain insight into the impact of alloy fluctuations on inter-well electron and hole transport properties. Therefore, we are interested in how carriers tunnel/transmit through an InGaN/GaN MQW with different barrier widths and with different "levels of randomness" in the wells (see below for details). To do so, we are focussing on ballistic transport calculations. To this end we start and end the simulation cell with InGaN regions. A schematic illustration of a typical simulation cell is given in Fig. 1. The left and right contacts are treated the same way as the MQWs being considered for transport calculations. This means, in a virtual crystal calculation (VCA) the contacts are described by a virtual crystal; if random alloy fluctuations are being considered in the well regions, the contacts are set up as a random alloy. We note that left and right contact exhibit always the same alloy configuration. In doing so, this approach ensures that the carriers populate the wells and that transmission properties can be studied efficiently, without having to include numerically expensive electron-phonon coupling effects, which can be addressed in future studies. We note that similar

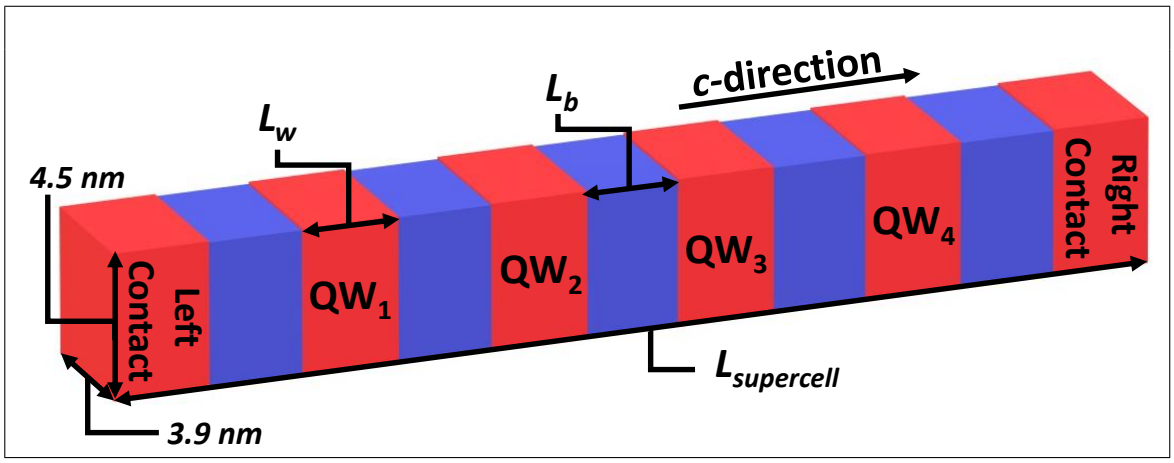

Figure 1: Schematic illustration of the supercell used in our ballistic transport calculations. Red indicates regions of $In_{0.12}Ga_{0.88}N$ and blue indicates regions of GaN.

approaches have been used in the literature to study the ballistic transport properties in InGaN MQWs, however, without considering the impact of alloy fluctuations and thus connected carrier localization effects [26–28].

To address the question of the impact of (random) alloy fluctuations on the ballistic transport properties of InGaN MQWs in detail, we proceed in the following way. As a starting point we describe the MQW system within VCA. Such an approach is similar to a three-dimensional continuum based model, where alloy fluctuations are not captured. Thus the assumption is that InGaN is a homogenous alloy that can be described by position independent averaged parameters. The results from the VCA calculations are then compared to an equivalent structure (e.g. same In content, same barrier width etc.) in which random alloy fluctuations are taken into account on a microscopic level.

We note that both VCA and calculations accounting for alloy fluctuations are performed on three-dimensional supercells. Such a set up leads to band folding effects. In the following we focus our attention on $\mathbf{K}_\parallel = \mathbf{0}$ states, where $\mathbf{K}_\parallel$ is the supercell in-plane k-vector. In the case of our VCA calculations where $\mathbf{k}_\parallel$, the in-plane wave function of the primitive cell, is a good quantum number, several states with different in-plane wavevectors are folded back to $\mathbf{K}_\parallel = \mathbf{0}$. In the (random) alloy case, due to the breaking of the translational invariance, the states can no longer be classified with a unique $\mathbf{k}_\parallel$. In principle band structures as a function of $\mathbf{K}_\parallel$ can be derived, but alloy fluctuations will again affect the band structure and thus the transport properties. By band unfolding methods, effective band structures for the "primitive" cell can be obtained. Previous theoretical studies on SiGe and AlGaAs systems have used effective band structures for random alloy supercells and compared the calculated transmission properties of these systems with VCA results [29, 30]. These data show that random alloy fluctuations affect the transmission properties, but that this is a general feature and applicable to all considered $\mathbf{K}_\parallel$- or $\mathbf{k}_\parallel$-states in a similar fashion. Therefore, to study the impact of alloy fluctuations on electron and hole ballistic transport in c-plane InGaN/GaN MQWs in

general, we consider in the following the situation of $\mathbf{K}_{\parallel} = \mathbf{0}$. To flesh out the influence of alloy fluctuations in detail, we vary also the "level of randomness" in the wells. How this is done is described in the following section, where the MQW model systems are introduced.

3. Model Systems

To study the impact of alloy fluctuations on electron and hole ballistic transport properties, we investigate different structures. First we focus our attention on fundamental aspects such as how the "level of randomness" in an InGaN MQW system affects the results. The supercells that underlie these studies are described in Sec. 3.1. In a second step, Sec 3.2, we turn our attention to systems that in terms of the number of QWs, well width and the presence of a $p-i-n$ junction induced electrostatic built-in field better resemble a device structure. Here, structures with the barrier widths L_b are considered, allowing us to analyze the impact of L_b on the ballistic carrier properties.

3.1. Varying levels of disorder in InGaN multi quantum well systems

We will first look at an $In_{0.12}Ga_{0.88}N$/GaN MQW system with two wells. The well width L_w and barrier width L_b are $L_w = L_b = 2.6$ nm. For our full 3-D calculation, a supercell with an in-plane area A of $A \approx 3.2 \times 2.8$ nm^2 and a height of $h \approx 18.1$ nm along the c-direction is generated; the cell contains 14,000 atoms. We have recently shown that the (in-plane) hole localization length in InGaN QWs with 10% is of the order of 2 nm [31]. Thus, the chosen in-plane dimensions are large enough to capture the (in-plane) localization length of holes; the out-of plane (along the c-axis) hole localization lengths are of similar length but are mainly determined by the built-in field along the growth direction, which is taken into account in our calculations.

In order to investigate the impact of (random) alloy fluctuations on inter-well transport in general, three different situations, in terms of how the QW region is described in the TB model, will be discussed. The aim is to compare results from calculations in which the "level of disorder" within the QWs varies. More specifically, the $In_{0.12}Ga_{0.88}N$ QWs will be described by

(i) a VCA - Any variation in local alloy composition is neglected.

(ii) a random distribution of In atoms in the InGaN well, but *both QWs* exhibit the *same In atom distributions* (same microscopic configuration). This system is labeled as "Random I".

(iii) a random distribution of In atoms in the InGaN well, but the QWs exhibit *different In atom distributions* (different microscopic configurations). This system is labeled as "Random II".

3.2. Interplay of barrier width and p-i-n junction field

While the supercells discussed above are designed to shed light on the impact of alloy disorder on ballistic transport properties in general, it is also important to analyze the impact of the barrier width and the electrostatic built-in field due to the presence of a $p-i-n$ junction on the results. Here, we consider an $In_{0.12}Ga_{0.88}N$ MQW system, embedded in a $p-i-n$ junction, with well widths of $L_w = 2.6$ nm. As already mentioned above, the field due to a $p-i-n$ junction is calculated within NextNano. [23] To do so, in NextNano the intrinsic region is set to a width of 55 nm and n- and p-contacts are modeled with constant doping density profiles of 5×10^{18} cm^{-3} and 2×10^{19} cm^{-3} respectively; similar doping concentrations have for instance been used in Ref. [32]. In the following we focus our attention on the equilibrium solution, meaning that no bias is applied. This set up is sufficient for our aim to gain first insight into the interplay of alloy fluctuations, barrier width and combined electrostatic field originating from intrinsic spontaneous, piezoelectric and $p-i-n$-junction induced fields.

Building on this framework, the transportcalculations are performed on supercells with an in-plane area A of $A = 4.5 \times 3.9$ nm^2, which again is large enough to capture hole localization effects. To study the impact of the barrier width L_b on the results, MQWs with two different barrier widths have been studied, namely $L_b = 3.1$ nm and $L_b = 5.2$ nm. The overall system size is therefore $4.5 \times 3.9 \times 28.8$ nm^3 (43,904 atoms) and $4.5 \times 3.9 \times 34.6$ nm^3 (59,584 atoms), respectively. While the approximation Random I is useful to establish general aspects, we do not study this situation here, since it is unlikely to be found in structures grown epitaxially. Thus we consider a VCA description of the wells and different random microscopic configurations in the wells (Random II, see above). To analyze the impact of the alloy microstructure in more detail, the calculations have been repeated five times, thus five different microscopic alloy configurations have been generated.

4. Results

Having discussed the theoretical framework and the model systems under consideration, we present here the results of our calculations. Before turning to transport results, in Sec. 4.1, we initially discuss general aspects of the electronic structure of InGaN/GaN MQWs and how it is affected by alloy fluctuations and electrostatic built-in fields. This information is important for understanding the observed transmission spectra of the different model systems. In Sec. 4.2 we present results on the impact of different levels of disorder on electron and hole ballistic transport. The impact of barrier width, alloy fluctuations and built-in field due to a $p-i-n$ junction on electron and hole transmission spectra are discussed in Section 4.3.

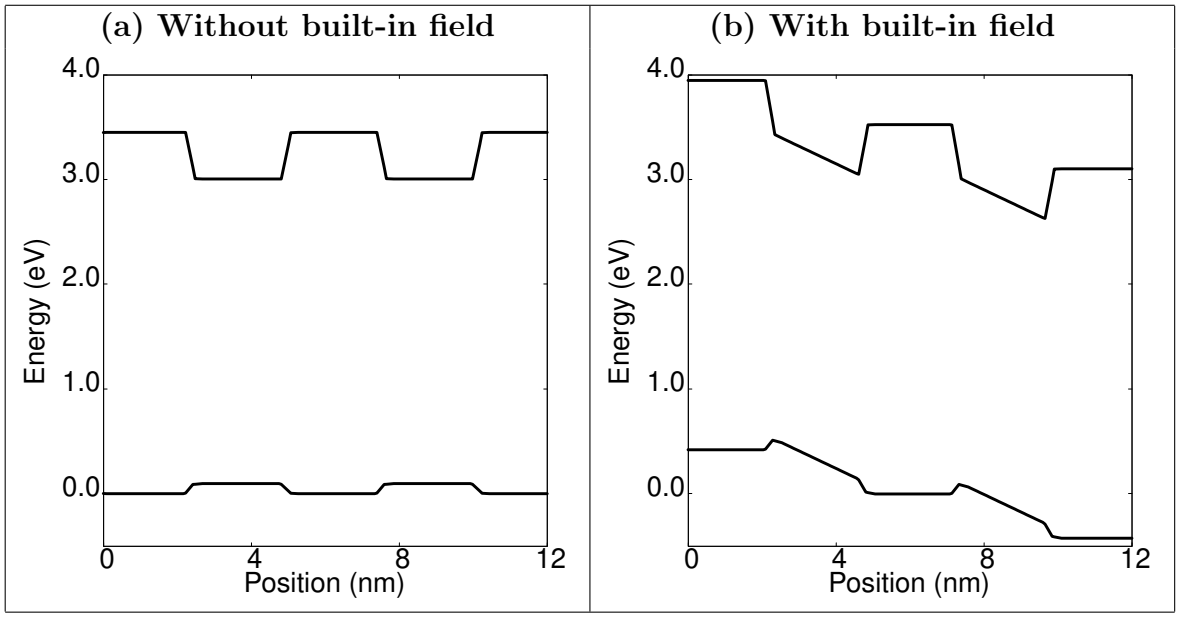

Figure 2: Conduction and valence band edges for a two $In_{0.12}Ga_{0.88}N$/GaN quantum well system described in a virtual crystal approximation. (a) Band edges in the absence of spontaneous and piezoelectric polarization induced built-in potentials. (b) Band edges in the presence of these built-in potentials.

4.1. Electronic structure of an InGaN/GaN MQW: VCA vs. Random Alloy

To establish general aspects of the impact of alloy fluctuations on the electronic structure in MQW systems, we study in the following the structures discussed in Sec. 3.1. The CBE and VBE profiles within VCA in the absence and the presence of the built-in field are shown in Fig. 2 (a) and (b) respectively. Comparing Fig. 2 (a) and (b) clearly shows that the built-in field breaks the symmetry of the otherwise identical wells. In the following, to disentangle effects stemming from the electrostatic built-in potentials (due to the spontaneous and piezoelectric polarization fields) and effects originating from the alloy microstructure, we first analyze results in the absence of the built-in field. Figure 3 shows isosurfaces of the electron (blue) and hole (red) ground state charge densities for (i) VCA, (ii) Random I and (iii) Random II systems viewed along the c-axis. This "top view" gives information about the charge density distribution within the c-plane. The isosurface corresponds to 40% of the respective maximum charge density values. Figure 3 also shows the planar-integrated charge density, $P(z_k)$, which is defined by

$$P(z_k) = \sum_{i,j} \sum_{\alpha} |c^{\alpha}_{ijk}|^2 \ , \tag{1}$$

given that the TB (electron or hole) wave function, Ψ, is expressed as:

$$\Psi = \sum_{i,j,k} \sum_{\alpha} c^{\alpha}_{ijk} \ \varphi^{\alpha}_{ijk} \ . \tag{2}$$

Here, i, j and k denote the x, y and z coordinates, respectively, of the N lattice sites in the supercell. The basis states of our sp^3 TB model are denoted by φ^{α}_{ijk}, with

$\alpha \in \{s, p_x, p_y, p_z\}$. The expansion coefficient at each lattice site is given by c^{α}_{ijk}. These coefficients are obtained by solving the eigenvalue problem for the Hamiltonian describing the MQW system, $\hat{H}\Psi = E\Psi$.

While the isosurface plots of the charge densities viewed along the c-axis provide insight into in-plane carrier localization effects, the planar-integrated probability density $P(z_k)$, Eq. (1), gives insight into carrier localization along the c-axis, e.g., in which QW the carriers are localized.

In a first step we turn our attention to the VCA results. Since in this case alloy fluctuations within the QW region are not captured, the electron and hole charge densities are distributed across the entire two QWs. This is clearly reflected in $P(z_k)$ shown in Fig. 3 (i). Turning to the system labeled as Random I, Fig. 3 (ii), in which case the alloy fluctuations are identical in both wells, the electron charge density is still well distributed across the two QWs, as $P(z_k)$ shows. However, some alloy fluctuation induced localization effects are visible in the different plots. Looking at the electron ground state first, we find an almost equal distribution of charge density in both wells. Due to the low effective electron mass, at least when compared to the holes, the electron wave functions of the two wells couple similar to the bonding and anti-bonding states in a homonuclear molecule. We find that this is also reflected in the calculated energy spectrum (not shown) where the first two electron states are energetically split and that this splitting is reduced with increasing barrier width between wells. Turning to the hole ground state, we find that alloy fluctuations lead to strong wave function localization effects. While we still observe significant charge densities in both wells, the ground state wave function is preferentially localized in QW 1. However, we note also that, as the wells contain the same microscopic configuration, there is a second hole state which is almost energetically degenerate with the state presented in Fig. 3 (ii); this second state has a slightly higher probability density in QW 2 (not shown). We attribute the smaller energetic separation of the first two hole states, when compared to the electrons, to a reduced electronic coupling between the two wells due to the larger hole mass and stronger hole localization effects when compared to electrons.

In Random II the picture changes noticeably. Now that the two wells differ in their microscopic alloy configuration, the symmetry of the system is broken and the ground state for electrons and holes are localized entirely within one well, as $P(z_k)$ clearly shows.

Having discussed the electronic structure of the three different systems in the absence of the electrostatic built-in field, Fig. 4 displays isosurface plots of the electron (red) and hole (blue) ground state charge densities along with planar integrated probability density, $P(z_k)$, in the presence of the field. The corresponding CBE and VBE profiles, within VCA, are shown in Fig. 2 (b). As Fig. 2 (b) reveals, the polarization potential leads to a significant tilt in the band edges; thus already in VCA the symmetry between the wells is broken by the built-in field. As a consequence the ground state for the electrons is always found in QW 2, while the hole ground states is found in QW 1. Comparing the electron and hole ground state charge densities from VCA, Random I and Random II, cf. Fig. 4, at least in terms of localization of these states along

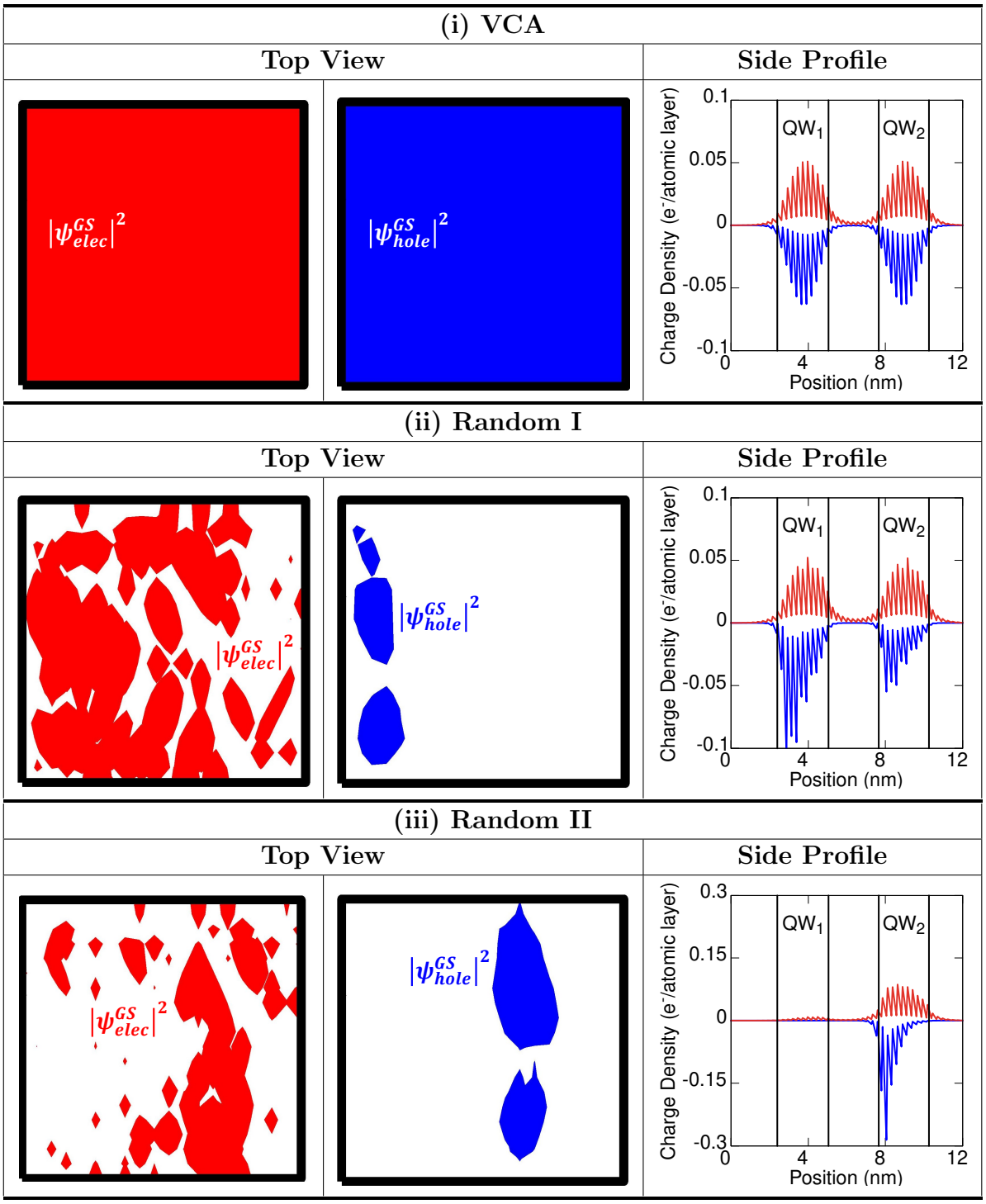

Figure 3: Top view (along the c-axis) of isosurface plots of (left) electron and (middle) hole charge densities for a (i) VCA, (ii) Random I and (iii) Random II system without the inclusion of the built-in polarization field. The isosurfaces correspond to 40% of the respective maximum charge density values. The right panel of the figure shows the planar integrated charge density, $P(z_k)$, along the supercell for both electrons and holes.

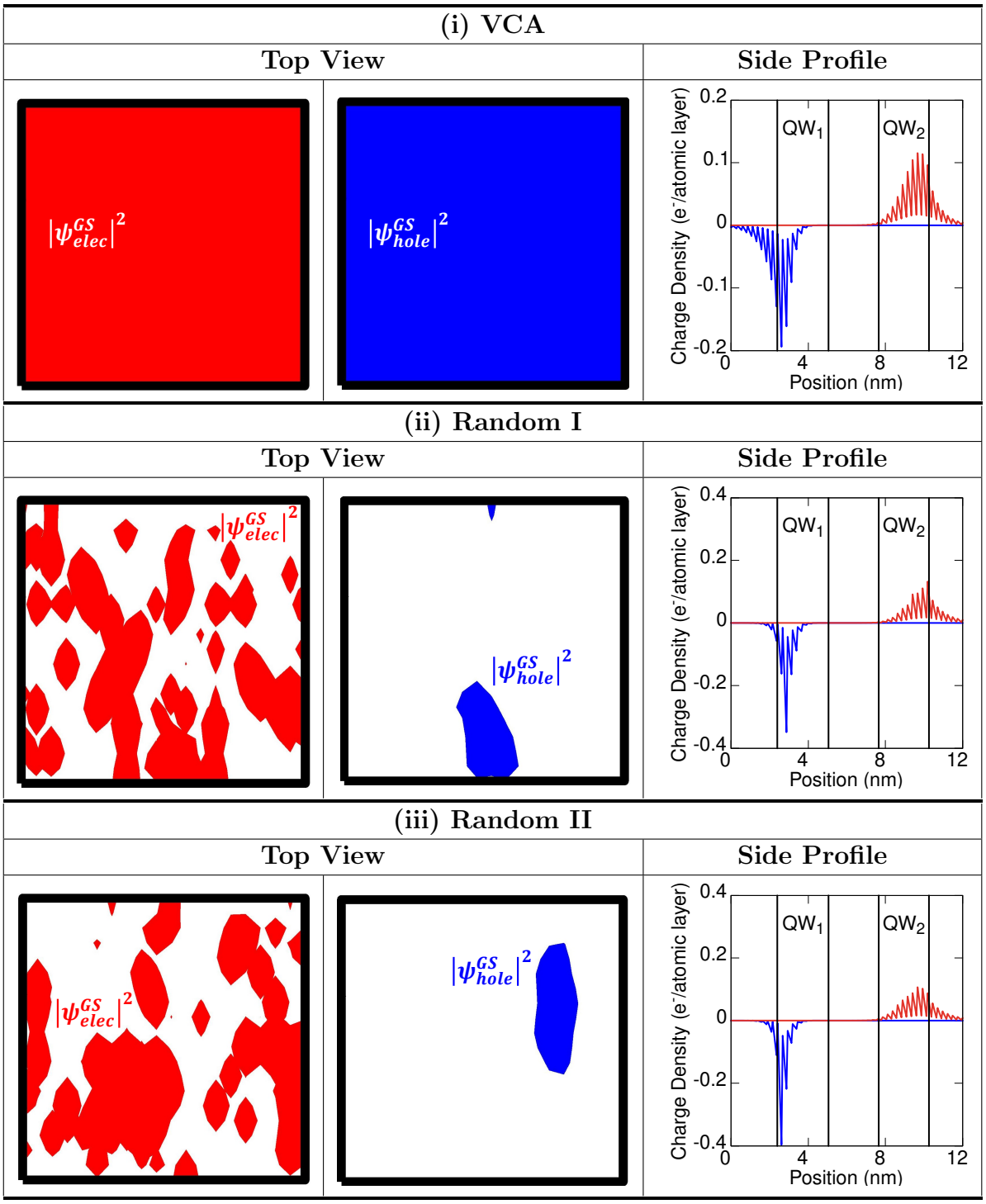

Figure 4: Top view (along the c-axis) of isosurface plots of (left) electron and (middle) hole charge densities for a (i) VCA, (ii) Random I and (iii) Random II system with the built-in polarization field included. The isosurfaces correspond to 40% of the respective maximum charge density values. The right panel of the figure shows the planar integrated charge density, $P(z_k)$, along the supercell for both electrons and holes.

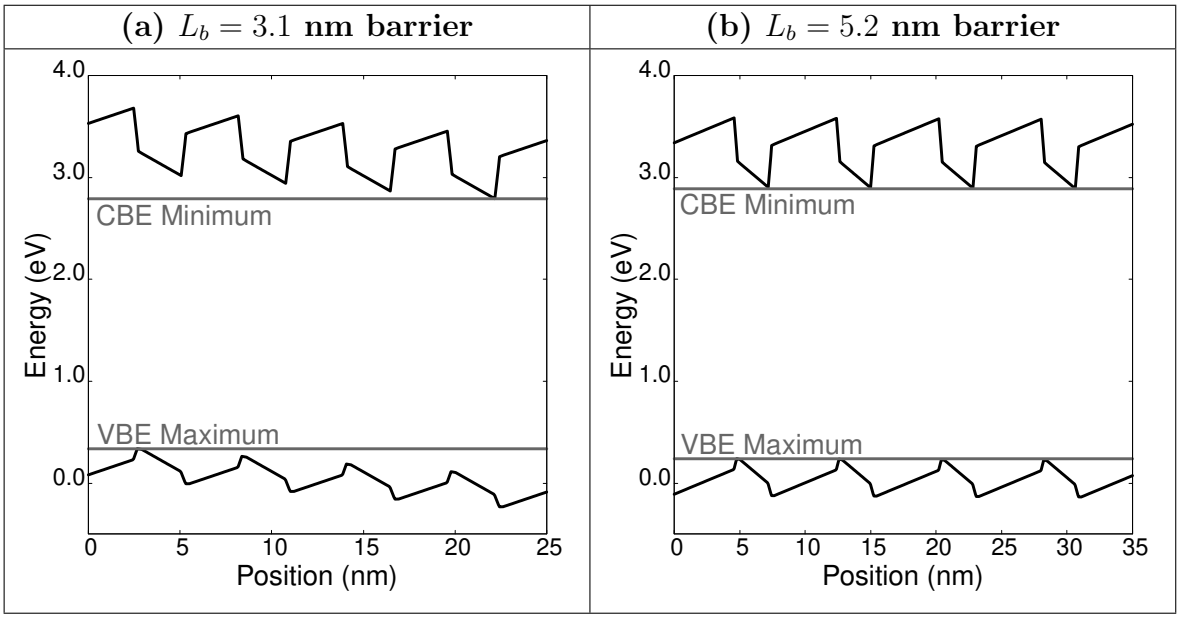

Figure 5: Conduction and valence band edges, in virtual crystal approximation, for the four $In_{0.12}Ga_{0.88}N$ multi quantum well system including a built-in field due to a $p-i-n$ junction, spontaneous and piezoelectric polarization effects. Band edge profile for a barrier width (a) of $L_b = 3.1$ nm and (b) of $L_b = 5.2$ nm.

the growth direction, the systems are not very different. However, it is important to highlight that in-plane localization effects are not captured in VCA and that the alloy microstructure will still affect carrier localization effects within the plane.

Having seen the impact of the spontaneous and piezoelectric polarization field induced built-in potential on the carrier confinement, we briefly discuss how the band edge profile is modified when the field of the $p-i-n$ junction is also present and the barrier width, L_b, between the wells is changed. Figure 5 shows the CBE and VBE profile of the four QW system discussed in Sec. 3.2 for the barrier width L_b of (a) L_b=3.1 nm and (b) $L_b = 5.2$ nm. The horizontal lines indicate the CBE minimum and the VBE maximum in the systems. In the system with $L_b = 3.1$ nm there is a clear difference in the CBE of the first (most left) QW and the last (most right) QW, thus a symmetry breaking between the wells in the MQW system is observed. In the case of $L_b = 5.2$ nm, the field of the $p-i-n$ junction "realigns" the CBEs of the four QWs. We note that these calculations are carried out for the same doping profiles; changes in the band edge profile arise entirely from changes in the barrier width. Below we discuss the effect of these changes in the band edge profile for transport properties. However, first, we focus our attention on the impact of the different levels of randomness on the transmission properties of the two QW systems discussed above.

4.2. Impact of alloy fluctuations on transmission properties of InGaN MQWs

In order to understand the impact of the underlying alloy microstructure on ballistic electron and hole transport, we start with the 2 QW system discussed above. Since we have already seen that the intrinsic built-in field significantly affects the electronic structure of this system, we follow the same procedure as above and neglect this potential initially; its impact on the results will be discussed in a second step.

4.2.1. Absence of built-in field Focusing on electrons/conduction band first, Fig. 6 (a) depicts the transmission spectrum of the two QW system in the absence of the built-in field when calculated within VCA (black) and Random I (blue). The results for Random I are averaged over 5 different random alloy configurations. In case of the VCA description (black), the transmission spectrum shows a doublet of peaks with transmission close to 1 below the GaN CBE of 3.45 eV. This doublet stems from the bonding/anti-bonding electron states in two QWs (see above). A similar situation is found for transmission peaks near the CBE of GaN ($\approx$ 3.45 eV). The larger splitting in energetically higher lying peaks stems from the effect that near the GaN CBE the electronic states from the two QW interact more strongly, resulting in a larger splitting of bonding and anti-boding states when compared to the energetically lower lying (more strongly bound) electron states. Also, the broadening of the peaks is related to the confinement of the states. Above the GaN CBE ($>$ 3.45 eV) there is a continuum of states which facilitate transmission. Turning to the results from the calculation within the Random I frame (blue), the spectrum is very similar to the VCA result. Figure 6 (a) also reveals that each microscopic configuration leads to transmission peaks at slightly different energetic positions. In general, this effect gives rise to a broadening of the energetic range over which transmission may be expected. Several things are important to note. First, the low transmission peak values at an energy of 3.2 eV in the Random I case result from averaging over the 5 different microscopic configurations and are *not* a result of the random alloy fluctuations in the well. For an individual configuration these peaks are sharp and they exhibit a transmission value of close to 1. This can be seen in Fig. 7 where the electron transmission spectrum of an arbitrary microscopic configuration is shown for Random I (blue). The same effect is seen at the energetically higher lying peaks, and the continuum above the GaN CBE. However, given that the peaks are sharp and their energies differ (slightly) between configurations, the averaging process reduces the heights of the peaks. This effect is less pronounced for higher lying peaks since these are broader and the variation in energy between different configurations is smaller. This analysis shows that, for electrons, the alloy fluctuations in the well do not lead to a (strong) reduction in the ballistic transport properties.

We note also that for the VCA description, assumptions about the parameter averaging procedure (e.g. bowing parameters) has to be made. Therefore, usually a reference/benchmark system is required. Having now the random alloy system as a reference, by adjusting the VCA further, a good agreement between VCA and Random

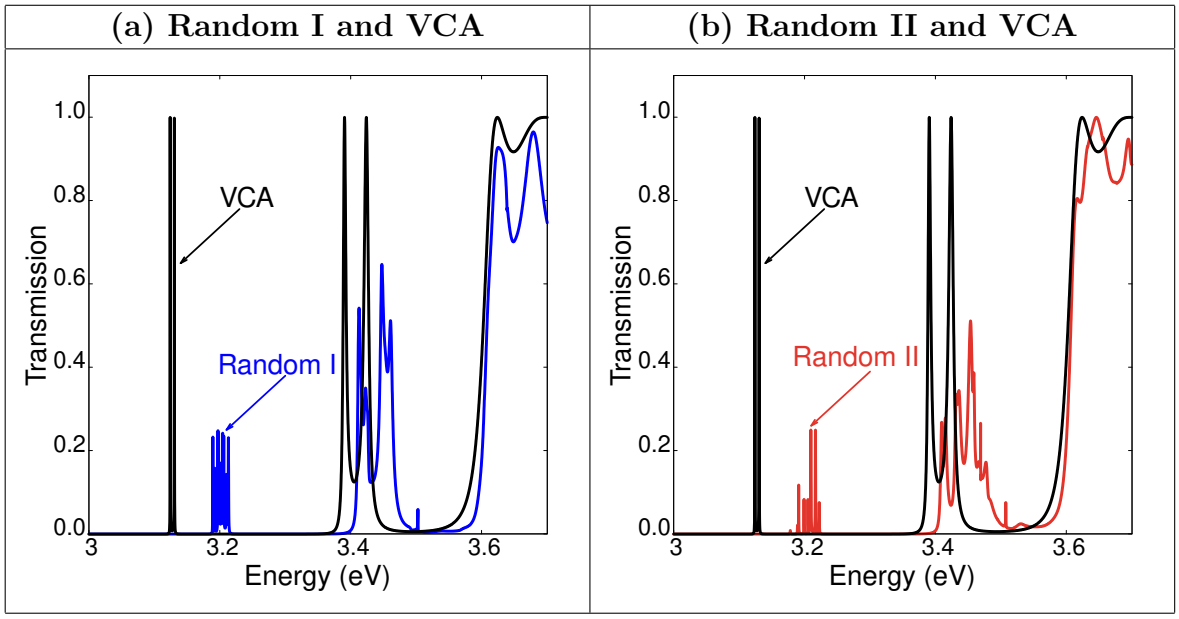

Figure 6: Electron transmission spectra through a two $In_{0.12}Ga_{0.88}N/GaN$ MQW system with well width of $L_w = 2.6$ nm and barrier width of $L_b = 2.6$ nm. The results are shown in absence of the built-in field. Virtual crystal approximation (VCA) results are given in black; random alloy system in blue and red, respectively, averaged over 5 microscopic configurations.

I may be achieved, given that the overall features of the transmission spectra are very similar.

So far we have assumed that the alloy microstructure in the two wells is the same. The question remains how the different random alloy configurations within the two wells will affect the transmission properties. Thus in the following we focus on the comparison between VCA and Random II.

Figure 6 (b) shows the transmission spectrum for the VCA (black) and the Random II (red) system. Overall, the spectrum within Random II is at, first glance, not very different from the spectrum calculated within Random I (cf. 6 (a)). Therefore the VCA spectrum also gives a good approximation of the Random II spectrum. However, now that the microscopic configuration differs between the two QWs, the symmetry between the wells is broken and the electronic states between the wells do not necessarily align energetically. As a result, the transmission of the lowest lying states is now indeed reduced. To see this clearly, Fig. 7 shows the transmission spectrum of an arbitrarily chosen microscopic configuration in Random II in comparison to the spectrum of Random I. While above the GaN CBE the two structures give basically the same spectrum, the transmission via bound QW states is noticeably reduced in the Random II case when compared to Random I. But, overall the electron transmission spectrum does not change dramatically between the two different random alloy assumptions and VCA gives a good description of the general features of the spectrum.

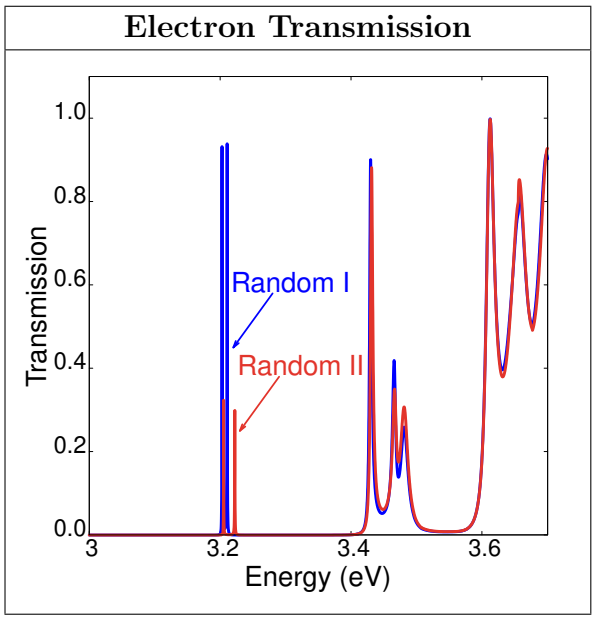

Figure 7: Comparison of the transmission properties of electrons for an arbitrary microscopic alloy configuration for Random I (blue) and Random II (red) in the $In_{0.12}Ga_{0.88}N/GaN$ MQW system with two wells; the well width $L_w = 2.6$ nm and the barrier width $L_b = 2.6$ nm. The calculations are performed in the absence of the built-in field. Random II differs from Random I by having a different microscopic alloy configuration in the second well, the alloy microstructure in the first well is identical in the two systems.

We now analyze the same situations for ballistic *hole* transport. Figure 8 (a) shows a comparison of the hole transmission spectra in VCA and Random I systems. The latter is again averaged over 5 different microscopic configurations. While for electrons, Random I and VCA gave very similar results, the hole spectra reveal a drastically different picture. Since the VBE of the unstrained GaN barrier is chosen as the zero of energy for the considered structures, cf. Fig. 2 (a), the VCA calculation shows one doublet of transmission peaks stemming from bound hole states in the well. As in the electron calculation, this doublet originates from the bonding and anti-bonding states of the two QWs within VCA. By comparison, the Random I case reveals a high density of transmission channels close to the GaN band edge, which are not present in the VCA result. We note also that Random I gives rise to new transmission peaks energetically above the VCA QW related transmission peaks. As a result, a continuum based calculation neglecting alloy fluctuations would underestimate the ballistic hole transport.

We attribute the appearance of extra transmission channels in the Random I case to the alloy induced symmetry breaking effects. Given the strong hole localization discussed in the literature [18, 31, 33] and also above, a significant deviation from an ideal QW picture may already be expected. While in the VCA/ideal QW case all well states can be

classified according to their in-plane **k**-vector, $\mathbf{k}_{\|}$, this classification is no longer possible for the random alloy case. So, $\mathbf{k}_{\|}$-vector conservation for transmission is no longer required in the random alloy case. As a consequence, the random alloy calculations include extra channels which are available to contribute to transmission. A similar argument has recently been put forward for optical properties, where it has been argued that the absence of $\mathbf{k}_{||}$ as a good quantum number results in more optically allowed transitions when compared to a VCA description of an InGaN QW [34]. Overall, our analysis shows that the VCA gives a poor estimate of hole ballistic transport properties, in contrast to electrons.

The question remains how the result is changed when the randomness is different in the two wells, which is reflected in our system labeled as Random II. The outcome of this analysis is shown in Fig. 8 (b). For Random II the transmission close to the GaN VBE is very similar to the Random I case and therefore noticeably different from the VCA results. However, the transmission peaks at energies higher then the energetically highest doublet in VCA are basically missing in Random II, which presents a difference to the Random I data (cf. Fig. 8 (a)). We relate this effect to the symmetry breaking between the wells. Even though the average In content is the same, the difference in the alloy microstructure leads to different electronic structures in the wells, given the pronounced hole localization effects. As a consequence, the transmission probability involving energetically higher lying (more strongly bound QW) states is reduced in the Random II case when compared to its Random I counterpart. This can be seen in Fig. 9 where the transmission spectrum of Random I (blue) and Random II (red) of an arbitrarily chosen configuration is shown. Above 0.015 eV, most peaks in Random II are smaller when compared to Random I. By contrast, the states closer to 0 eV (unstrained GaN VBE) are more delocalized wave functions so that the electronic coupling between the wells is stronger and in turn a higher transmission probability is observed. Along with the breakdown of $\mathbf{k}_{\|}$ as a good quantum number, a larger number of transmission peaks is observed in Random I and II when compared to VCA.

Overall, our analysis shows that changing the randomness between the wells has a slight impact on the hole transmission spectrum. Introducing random alloy fluctuations in general is the dominant effect as seen above. But, in addition to the symmetry breaking of the random alloy fluctuations, the presence of the electrostatic built-in field will also have a strong impact. We study its impact on the electron and hole ballistic transport properties in the following section.

4.2.2. Impact of the Built-in field Including the polarization field results in a potential step across the QWs (cf Fig. 2 (b)), which modifies the GaN CBE and VBE profiles. Therefore, the energy at which states are present to contribute to the transmission through the two QWs is changed.

Before looking at the fine details, Fig. 10 (a) shows that for electrons the transmission spectrum obtained within VCA reflects the same behavior as the spectrum obtained from Random I. Also, when comparing the Random II result with the VCA

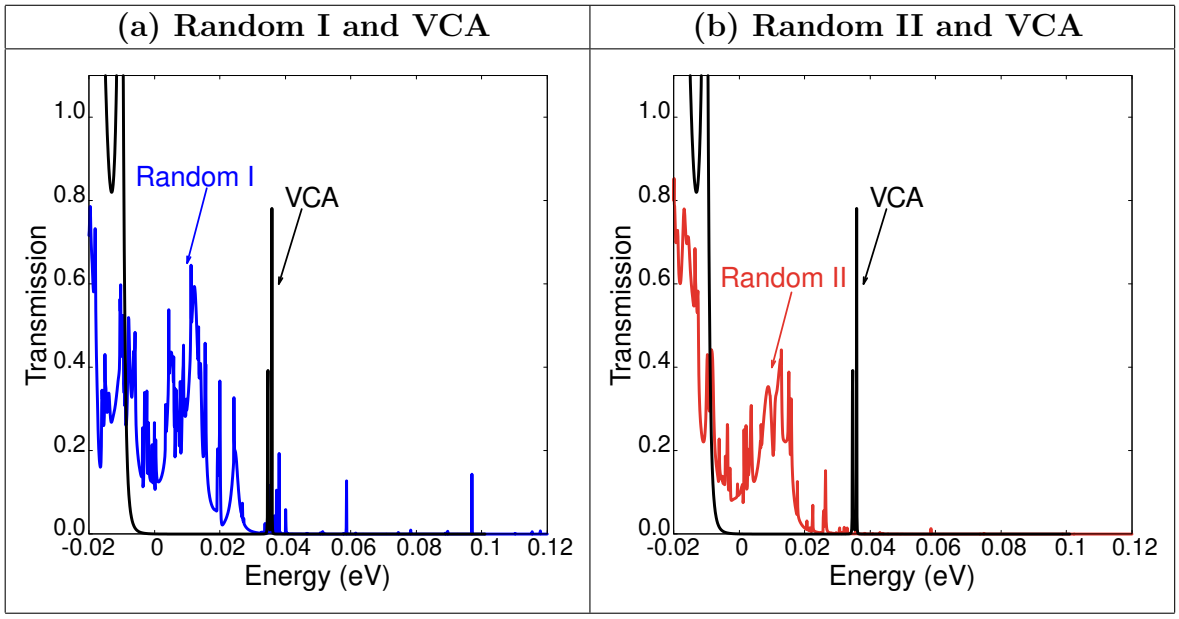

Figure 8: Hole transmission spectra through a two $In_{0.12}Ga_{0.88}N/GaN$ MQW system with well width of $L_w = 2.6$ nm and barrier width of $L_b = 2.6$ nm. The results are shown in the absence of the built-in field. Virtual crystal approximation (VCA) results are given in black; random alloy system in blue and red, respectively, averaged over 5 microscopic configurations.

data, as displayed in Fig. 10 (b), the spectra are very similar. We do not see a reduction in transmission peaks when the microscopic configurations are varied between the wells. Thus the transmission properties in this case are basically dominated by the electrostatic built-in field and not the random alloy fluctuations.

The same is true for holes, as the calculated transmission spectra depicted in Fig. 11 reveal. Thus, when taking the electrostatic built-in field into account, the VCA provides a good description of ballistic transport properties for both electrons and holes. However, it is important to note that in the flat band condition (no field), as discussed in the previous section, the situation especially for the holes is different. As we have seen in Sec. 3, the symmetry breaking between the wells due to the built-in field also depends on the barrier width between the wells and the presence of the $p-i-n$ junction induced field. Thus, we study in the following section how the presence of this external field in a device and changes in the barrier width affect the ballistic transport of electrons and holes in an InGaN MQW system.

4.3. Multi-quantum well system in a p-i-n junction

As already highlighted in Sec. 3, the built-in potential originating from the $p-i-n$ junction affects the CBE and VBE profile of a InGaN/GaN MQW system. Also we have discussed that the barrier width L_b in conjunction with this field will affect the band edge profiles. In the following sections we analyze their combined impact on the

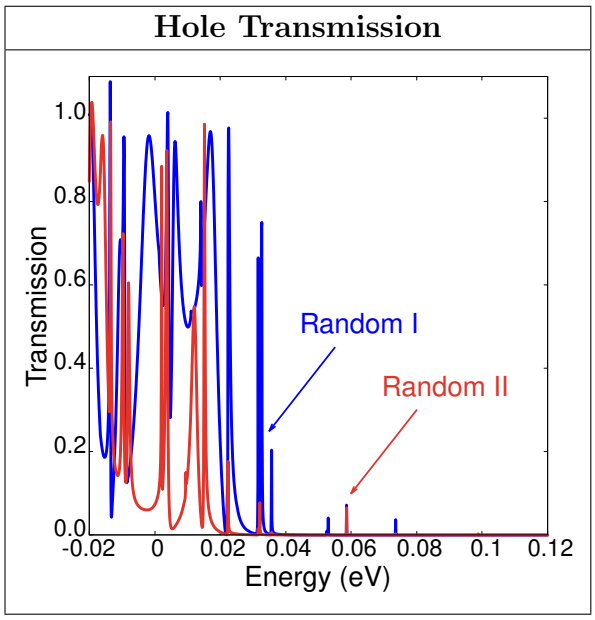

Figure 9: Comparison of the transmission properties of holes for an arbitrary microscopic alloy configuration for Random I (blue) and Random II (red) in the $In_{0.12}Ga_{0.88}N/GaN$ MQW system with two wells; the well width $L_w = 2.6$ nm and the barrier width $L_b = 2.6$ nm. The calculations are performed in the absence of the built-in field. Random II differs from Random I by having a different microscopic alloy configuration in the second well; the alloy microstructure in the first well is identical in the two systems.

ballistic transport properties of the MQW system introduced in Sec. 4.3.1. We start in Sec. 4.3.1 with the system with a barrier width of $L_b = 3.1$ nm before turning to the structure with $L_b = 5.2$ nm in Sec. 4.3.2. The width of the individual wells is kept constant at $L_w = 2.6$ nm.

4.3.1. Barrier width $L_b = 3.1$ nm The transmission spectrum calculated within VCA (black) and the Random II assumption (red) is shown in Fig. 12 for (a) electrons and (b) holes for the four $In_{0.12}Ga_{0.88}N/GaN$ MQW system with a barrier width of $L_b = 3.1$ nm. The random alloy data is obtained as an average over the transmission spectra of 5 different random alloy configurations. Looking at the VCA results for electrons first, Fig. 12 (a), transmission is mainly found at higher energies (> 3.5 eV). Below 3.5 eV the VCA transmission probability is low. Examining the CBE profile depicted in Fig. 5 (a) indicates that in the VCA case, bound QW states do not contribute to the transmission through the MQW system. In VCA, a similar situation is found for the holes, as Fig. 12 (b) reveals. Here, the first peak in the VCA hole transmission spectrum is found at around -0.13 eV. Looking at the VBE profile depicted in Fig. 5 (a), in terms of the energy, mainly the fourth well (last well on the right in Fig. 5 (a)) presents a potential barrier for the transmission process. Energetically higher lying valence states (bound hole states) do not contribute to the transmission, given that due to their high

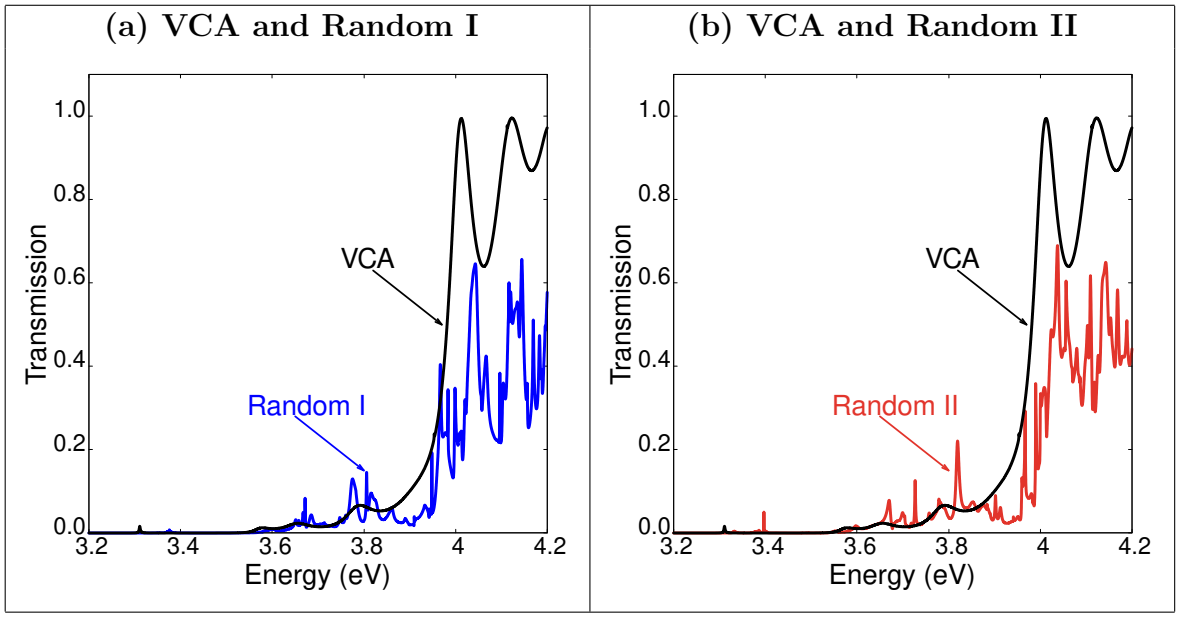

Figure 10: Electron transmission spectra through a two $In_{0.12}Ga_{0.88}N/GaN$ MQW system with well width of $L_w = 2.6$ nm and barrier width of $L_b = 2.6$ nm. The electrostatic built-in field is included in the calculations. Virtual crystal approximation (VCA) results are given in black, random alloy system in blue and red, respectively, averaged over 5 microscopic configurations.

effective mass, these wave functions are strongly localized within individual wells.

Turning to the random alloy case, and focussing initially on the electron transmission spectrum (cf. Fig. 12 (a)), the calculated spectrum is very similar to the VCA case. This means one is also left with very low transmission probabilities below 3.5 eV; only for energies larger than 3.5 eV significant transmission is observed. The difference between the random alloy case (red) and the VCA result in this energy range is the spectral broadening of the transmission. The VCA transmission is described by 2 distinct peaks before the onset of a continuum. By contrast, the random alloy calculation results in many peaks distributed across the same energy range (between 3.5 eV and 3.7 eV), before the continuum onset. These result from the differing microscopic configurations providing higher-probability transmission channels at different energies.

The situation is different for the holes. Figure 12 (b) shows, in addition to the VCA spectrum (black), also the hole transmission spectrum (red) of the Random II case. The comparison between VCA and Random II data reveal clearly that in the random alloy case an earlier onset (higher energies) of the transmission occurs. More specifically, we observe strong transmission peaks in the energy range from -0.1 eV to 0 eV in the random alloy calculation; VCA basically shows no peaks in this energy range. We again note that due to the averaging process, and the sharpness of the peaks, these peaks are a lower bound of the transmission in this energy range. In other words, a noticeable effect is observed due to the presence of random alloy fluctuations.

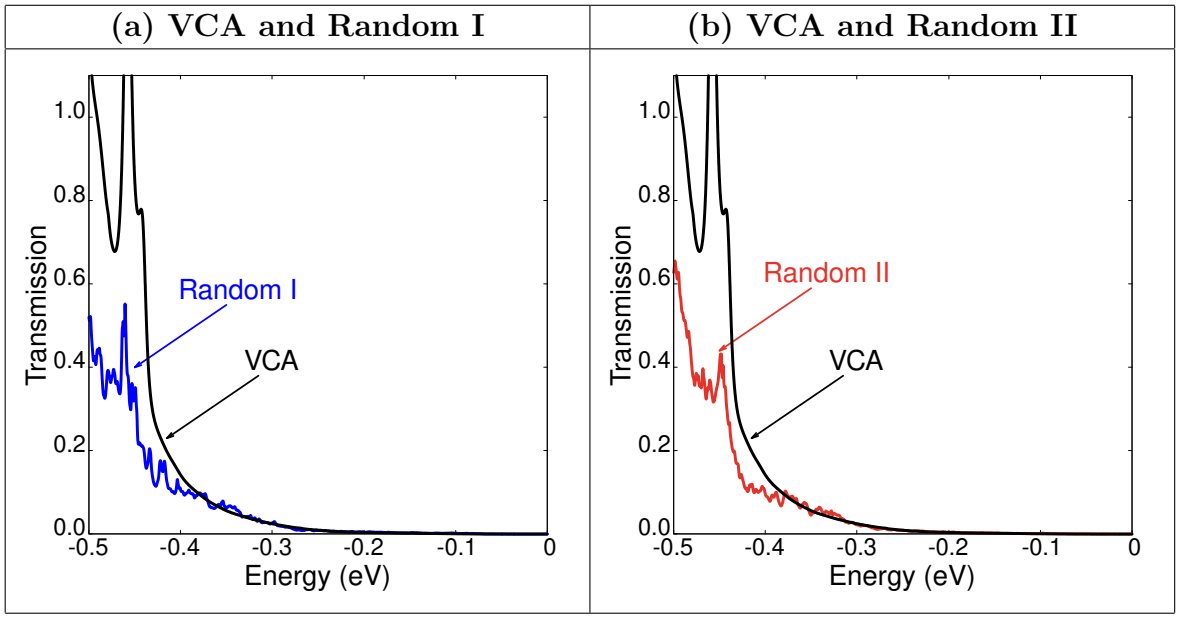

Figure 11: Hole transmission spectra through a two $In_{0.12}Ga_{0.88}N$/GaN MQW system with well width of $L_w = 2.6$ nm and barrier width of $L_b = 2.6$ nm. The electrostatic built-in field is included in the calculations. Virtual crystal approximation (VCA) results are given in black, random alloy system in blue and red, respectively, averaged over 5 microscopic configurations.

Overall, this investigation reveals that (i) the energetic alignment of the different wells in a MQW system becomes important for the transmission probability of the carriers, (ii) VCA gives a good description of the electron ballistic transport properties of the MQW system and (iii) that VCA underestimates the hole ballistic transport noticeably. Especially the last point is important. For efficient radiative recombination in an InGaN/GaN MQW system, the carriers ideally transfer easily between the wells so that when electrons are injected from the n-side and holes from the p-side of the device, all QWs in the MQW structure contribute to the light emission process. Therefore, the finding that the random alloy fluctuations introduce additional channels at lower energies would then facilitate a more efficient distribution of holes between the MQW system than expected from a VCA type calculation.

Overall alloying the GaN barrier with a small portion of In (e.g. 5%) could provide a pathway for improving hole transport in InGaN MQW systems and thus the carrier distribution in the different wells. Firstly, such an approach would reduce the effective barrier height, which results in weaker confinement of bound states and an increased leakage of carrier wave functions into the barrier. Secondly, InGaN barriers with low In content could also facilitate percolation transport between the wells. Here carriers can take a path through regions where the potential barrier is locally low. Similar effects have been observed for $n - i - n$ transport studies containing AlGaN electron blocking layers [35]. However, the impact of alloying the barrier with small fractions

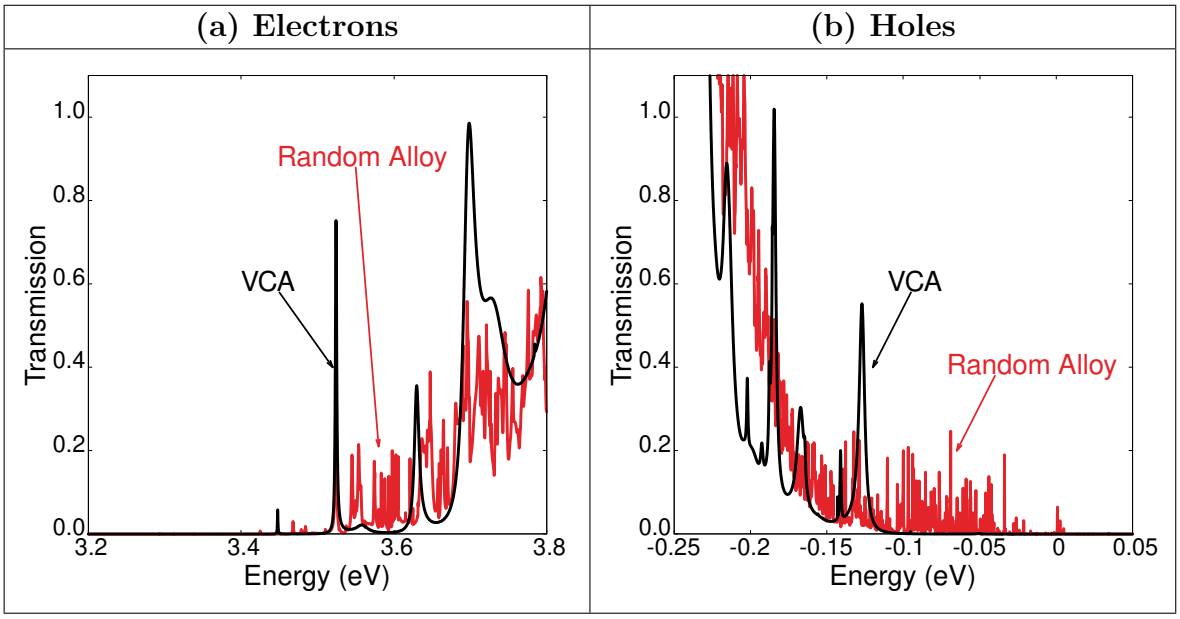

Figure 12: Transmission spectra of the four $In_{0.12}Ga_{0.88}N$/GaN MQW with well width of $L_w = 2.6$ nm and barrier width $L_b = 3.1$ nm calculated within virtual crystal approximation (black) and a random alloy description (Random II; red, averaged over 5 configurations). The calculations include spontaneous and piezoelectric built-in potentials as well as a field originating from a $p-i-n$ junction.

of In on the ballistic hole transport between wells may be more subtle. In the absence of alloy disorder, $\mathbf{k}$ is a good quantum number in the GaN barrier, so that there is no scattering once the carrier enters the barrier. In the presence of alloy fluctuations, scattering is possible and the transmission probability should be reduced. However, while this may be true for individual transmission peaks, a large number of additional channels may be made available. This is also reflected in our results above, which indicate that transmission above the GaN band edge is increased by alloy fluctuations. A similar feature has been observed in recent studies on the radiative recombination rates in InGaN/GaN QWs, where alloy fluctuations reduce the oscillator strength of individual transitions when compared to a VCA calculation. However, due to the breaking of the k-selection rules, the number of allowed transitions is increased, leading to an overall increase in the radiative recombination rate when compared to the VCA calculations [34]. We revisit the discussion of the potential impact of alloying the barrier material with In further below and present initial results in an appendix.

Here, we have discussed the ballistic transport properties for a barrier width of $L_b = 3.1$ nm. As we have seen above, cf. Fig. 5, the barrier width will also affect the VBE and CBE profile. Additionally the electronic coupling between the wells, and therefore the ballistic transport, should also be affected by the barrier width. In the next section we analyze the impact of L_b on the transmission properties in more detail.

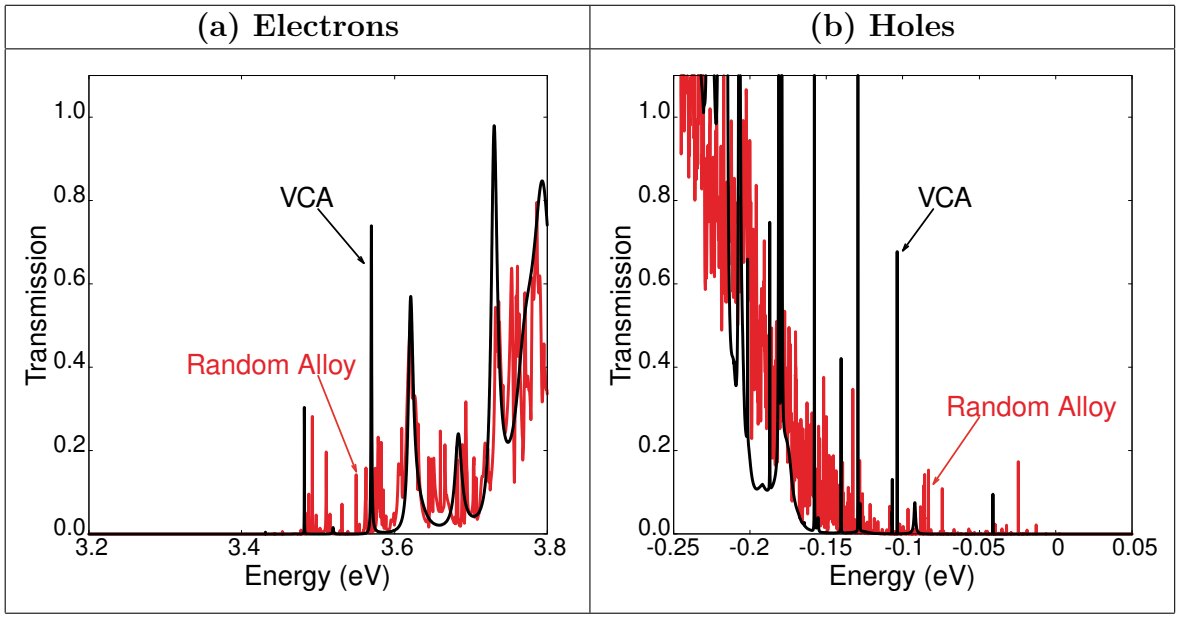

Figure 13: Transmission spectra of the four $In_{0.12}Ga_{0.88}N$/GaN MQW with well width of $L_w = 2.6$ nm and barrier width $L_b = 5.2$ nm calculated within virtual crystal approximation (black) and a random alloy description (Random II; red, averaged over 5 configurations). The calculations include spontaneous and piezoelectric built-in potentials as well as a field originating from a $p-i-n$ junction.

4.3.2. Barrier width $L_b = 5.2$ nm Figure 13 (a) shows the electron transmission spectra in VCA (black) for the $In_{0.12}Ga_{0.88}N$/GaN MQW system introduced in Sec. 3.2 with a barrier width of $L_b = 5.2$ nm; the spectrum obtained within the random alloy description Random II is given in red. The depicted data for Random II is the average over 5 different random alloy configurations. Bearing in mind the band edges in Fig. 5 (b), and looking first at the VCA data, we mainly observe transmission peaks above 3.6 eV, which is the CBE of the barrier material. Basically the same behavior is observed in the random alloy case. Thus, similar to the smaller barrier width discussed above, for electron ballistic transport, VCA yields a good description of the system.

Figure 13 (b) depicts the transmission spectrum for holes in VCA (black) and Random II (red). When comparing the calculated spectra for VCA and random alloy description, we find that the random alloy fluctuations introduce "extra" transmission channels when compared to VCA data. We note also that for the chosen barrier width, the CBE and VBE of the different wells are almost perfectly aligned in the VCA case. This is obviously the best case scenario, but is probably not the norm when e.g. changing doping profile or the barrier width further. Even a slight shift in the energies between neighboring wells results in a sharp reduction of the VCA transmission peaks (not shown). For the random alloy system the situation is different. Here, alloy fluctuations already break the symmetry between wells intrinsically, thus aligning or not aligning the band edges is of secondary importance for the random alloy case.

Bearing in mind the strong dependence of the VCA transmission on the alignment of the band edges, the random alloy fluctuations should still open additional transmission channels, given that **k**-conservation breaks down, and thus lead to an enhancement of the transmission. However, overall we can conclude that the wider barrier width suppresses ballistic transport compared to the narrower barrier width, given that electronic coupling between the QWs is reduced.

But, as discussed already above, alloying the barrier with In could provide a way forward to increase the transmission probability. Our calculations have shown that the hole transmission through the "extra" channels is sensitive to the state confinement, and the coupling between states in neighboring wells. Including In in the barrier would reduce the confinement of states within the wells, and could lead to a situation where hole ballistic transport is improved at wider barrier widths. In a recent experimental study, Marcinkevičius *et al.* analyzed such a situation [36]. Their data reveal indeed an increased hole transmission through an InGaN MQW system when 5% In was introduced in the GaN barrier. Our analysis indicates a potential mechanism underlying the experimentally observed increase in ballistic hole transport, which is supported by initial results presented in an appendix. Further studies are required to shed more light on this question; this is beyond the scope of the present study, which is aimed at providing insight into the impact of alloy fluctuations within the well and how the level of randomness affects the carrier transport in InGaN/GaN MQW systems.

5. Conclusion

In this work we have presented an analysis of the ballistic transport properties of InGaN/GaN MQW systems by means of a combined atomistic tight-binding non-equilibrium Green's function approach. We have paid special attention to the impact of (random) alloy fluctuations on both electron and hole ballistic transport. To investigate the impact of alloy disorder, results are compared to the outcome of calculations that utilize a virtual crystal approximation of the InGaN MQWs. Our data shows that for electrons the alloy microstructure is of secondary importance for their ballistic transport, while for hole transport the situation is different. We observe that for narrow GaN barrier width in an InGaN/GaN MQW system, the presence of the alloy fluctuations give rise to extra hole transmission channels when compared to a virtual crystal description of the same system. We attribute this effect to the situation that in the random alloy case, $\mathbf{k}_{\parallel}$-vector conservation is broken/relaxed and therefore the ballistic hole transport increases. Thus, a VCA description would underestimate the contribution from hole ballistic transport in general. However, for wider barrier width this effect is strongly reduced. Overall, our theoretical findings of significant ballistic hole transport for narrower barrier width, which decreases with increasing barrier width, is consistent with recent experimental studies [16].

Furthermore, the gained insight indicates a potential explanation for the recent experimental observation that alloying the GaN barrier region between the wells with

small fractions of In (e.g. 5%) is beneficial for hole ballistic transport in InGaN MQW system. Based on our results, such an approach results in (i) the breakdown of $\mathbf{k}_{\|}$-vector conservation and (ii) a slight reduction in the barrier height between the wells. As a consequence, especially the holes may become more evenly distributed between the different wells. Thus a larger number of wells can contribute to the light emission process and improve therefore the efficiency of the corresponding device.

Acknowledgments

The authors acknowledge financial support from Science Foundation Ireland under Grants No. 17/CDA/4789, No. 15/IA/3082 and No. 12/RC/2276 P2.

Appendix: Alloyed Barrier Material

As discussed above, alloying the barrier material could provide a pathway to enhance the ballistic transport in InGaN MQW systems. To analyze the potential impact of In in the barrier on the transmission spectrum for electrons and holes, we focus in the following on a 2 QW $In_{0.12}Ga_{0.88}N$ system. The system is generated in the Random II setting, where the microscopic configuration between the QWs differs.

We compare an $In_{0.12}Ga_{0.88}N$/GaN system to an $In_{0.12}Ga_{0.88}N/In_{0.05}Ga_{0.95}N$ system. The barrier is also treated as a random alloy which differs between each region of $In_{0.05}Ga_{0.95}N$. Here the barrier and the well width are both 2.6 nm. The QW configuration is kept fixed, so only the barrier material is changed for this comparison. We only consider one microscopic configuration in each case, so no averaging is done to obtain the results.

For the sake of simplified discussion, we neglect strain and polarization fields. When alloying the GaN barrier with 5% In, the CBE is shifted downwards from 3.45 eV (pure GaN) to approximately 3.36 eV ($In_{0.05}Ga_{0.95}N$) in the barrier region of the MQW system. Also the VBE of the barrier material changes: for pure GaN barriers, the VBE is chosen to be at 0 eV; in the case of 5% In in the barrier region, the VBE then shifts to approximately 0.03 eV.

Figure 14 (a) shows the electron transmission spectrum of the system with the pure GaN barrier (black) along with the spectrum obtained for an $In_{0.12}Ga_{0.88}N/In_{0.05}Ga_{0.95}N$ MQW structure (blue). With pure GaN barriers, transmission through the electron ground states (transmission peaks around 3 eV) is weak, while in case of the $In_{0.05}Ga_{0.95}N$ barrier, the ground state transmission is strongly enhanced. The effect of enhanced QW ground state transmission is accompanied by a slight red shift of the transmission peaks. We attribute both effects (red shift, enhanced transmission) to changes in carrier confinement in case of the alloyed barrier when compared to the pure GaN system. Similar effects are observed for the excited QW states at approximately 3.2 eV.

Figure 14 (b) depicts the results for the hole transmission. Our calculations show that the $In_{0.05}Ga_{0.95}N$ barrier significantly increase the ballistic hole transport facilitated

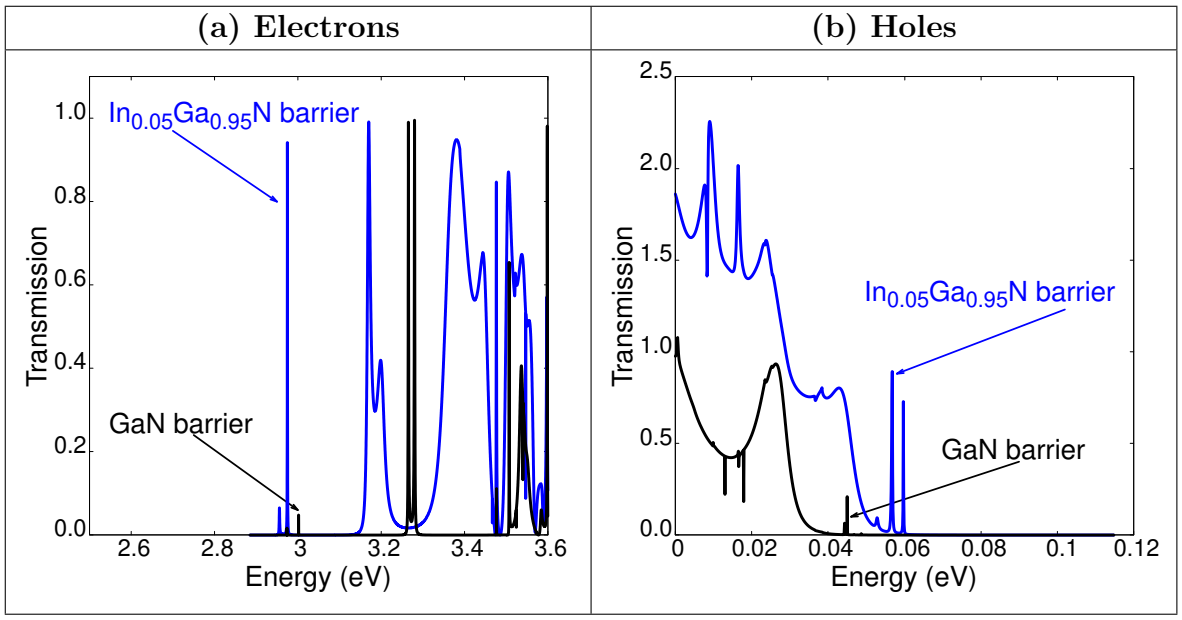

Figure 14: Transmission spectra of a 2 $In_{0.12}Ga_{0.88}N$ QW system with GaN (black) and $In_{0.05}Ga_{0.95}N$ (blue) barriers for (a) electrons and (b) holes. The microscopic configuration differs between the QWs but is kept the same for the pure GaN and the InGaN barrier. Thus only the barrier material differs between the two systems. Strain and built-in fields are not considered. The barrier and well width are $L_b = L_w = 2.6$ nm.

by QW confined states near energies of 0.06 eV. Also, and in comparison with the pure GaN barriers, transmission in the energy range of 0.03 eV to 0.05 eV is also increased significantly. We attribute this effect again to the reduction in the carrier confinement when comparing pure GaN and $In_{0.05}Ga_{0.95}N$ barriers.

Overall, these initial studies indicate that using InGaN barriers with low In content are beneficial for increasing the ballistic transport in InGaN MQW systems, and thus potentially enabling an improved distribution of carriers between the different QWs in a MQW structure. This finding may explain the experimental observation made in the work by Marcinkevičius *et al.* [16]. To shed further light on the influence of InGaN barriers on the transport properties of InGaN MQWs, future studies may target a variety of different questions. For instance, the question remains if there is a critical barrier In content at which alloy scattering will have a detrimental effect on the ballistic transport. Furthermore, we have followed here the experimental work of Ref. [16] and kept the In content in the well constant while increasing the In content in the barrier. As discussed above, this will reduce the carrier confinement. To disentangle effects arising from alloy fluctuations in the barrier and the barrier height (carrier confinement), investigations may be performed in which the relative band offset difference is kept constant, e.g. comparing transport properties of an $In_{0.12}Ga_{0.88}N$/GaN MQW system to the properties of an $In_{0.17}Ga_{0.05}N/In_{0.05}Ga_{0.95}N$ MQW structure. Such a detailed

and extensive analysis can be targeted in future investigations, which may focus on the impact of alloy fluctuations in the barrier material on the ballistic carrier transport. However, this is beyond of the scope of the present study, where our main aim is to understand the impact of alloy fluctuations within the well on transport properties.

References

[1] C. J. Humphreys, "Solid-State Lighting, The nature of carrier localisation in polar and nonpolar InGaN/GaN quantum wells," *MRS Bulletin*, no. 4, p. 459470, 2008.

[2] M.-H. Kim, M. F. Schubert, Q. Dai, J. K. Kim, E. F. Schubert, J. Piprek, and Y. Park, "Origin of efficiency droop in GaN-based light-emitting diodes," *Applied Physics Letters*, vol. 91, no. 18, p. 183507, 2007.

[3] J. Xu, M. F. Schubert, A. N. Noemaun, D. Zhu, J. K. Kim, E. F. Schubert, M. H. Kim, H. J. Chung, S. Yoon, C. Sone, and Y. Park, "Reduction in efficiency droop, forward voltage, ideality factor, and wavelength shift in polarization-matched GaInN/GaInN multi-quantum-well light-emitting diodes," *Applied Physics Letters*, vol. 94, no. 1, p. 011113, 2009.

[4] J. Piprek, "How to decide between competing efficiency droop models for GaN-based light-emitting diodes," *Applied Physics Letters*, vol. 107, no. 3, p. 031101, 2015.

[5] J.-R. Chen, Y.-C. Wu, S.-C. Ling, T. ko, T.-c. Lu, H.-C. Kuo, Y.-K. Kuo, and S.-C. Wang, "Investigation of wavelength-dependent efficiency droop in InGaN light-emitting diodes," *Applied Physics B*, vol. 98, pp. 779–789, 03 2010.

[6] R.-M. Lin, M.-J. Lai, L.-B. Chang, and C.-H. Huang, "Effect of an asymmetry AlGaN barrier on efficiency droop in wide-well InGaN double-heterostructure light-emitting diodes," *Applied Physics Letters*, vol. 97, no. 18, p. 181108, 2010.

[7] D. Browne, B. Mazumder, Y.-R. Wu, and J. Speck, "Electron transport in unipolar InGaN/GaN multiple quantum well structures grown by NH3 molecular beam epitaxy," *Journal of Applied Physics*, vol. 117, p. 185703, 05 2015.

[8] P. McBride, Q. Yan, and C. Van de Walle, "Effects of In profile on simulations of InGaN/GaN multi-quantum-well light-emitting diodes," *Applied Physics Letters*, vol. 105, pp. 083507–083507, 08 2014.

[9] K. Bulashevich, O. Khokhlev, I. Evstratov, and S. Karpov, "Simulation of light-emitting diodes for new physics understanding and device design," *Proceedings of SPIE - The International Society for Optical Engineering*, vol. 8278, pp. 18–, 02 2012.

[10] S. Karpov, "Modeling of III-nitride Light-Emitting Diodes: Progress, Problems, and Perspectives," *Proc SPIE*, vol. 7939, 02 2011.

[11] C. S. Xia, W. D. Hu, C. Wang, Z. F. Li, X. S. Chen, W. Lu, Z. M. Simon Li, and Z. Q. Li, "Simulation of InGaN/GaN multiple quantum well light-emitting diodes with quantum dot model for electrical and optical effects," *Optical and Quantum Electronics*, vol. 38, pp. 1077–1089, 2006.

[12] Chen, J.-R and Ling, S.-C and Huang, H.-M and Su, P.-Y and ko, Tongkyun and Lu, Tien-chang and Kuo, Hao-Chung and Kuo, Y.-K and Wang, Sun-Chong, "Numerical study of optical properties of InGaN multi-quantum-well laser diodes with polarization-matched AlInGaN barrier layers," *Applied Physics B: Lasers and Optics*, vol. 95, pp. 145–153, 01 2009.

[13] C. Sheng Xia, Z. M. Simon Li, W. Lu, Z. Hua Zhang, Y. Sheng, and L. Wen Cheng, "Droop improvement in blue InGaN/GaN multiple quantum well light-emitting diodes with indium graded last barrier," *Applied Physics Letters*, vol. 99, no. 23, p. 233501, 2011.

[14] C.-K. Li, M. Piccardo, L.-S. Lu, S. Mayboroda, L. Martinelli, J. Peretti, J. Speck, C. Weisbuch, M. Filoche, and Y.-R. Wu, "Localization landscape theory of disorder in semiconductors. III. Application to carrier transport and recombination in light emitting diodes," *Physical Review B*, vol. 95, 04 2017.

[15] T.-J. Yang, R. Shivaraman, J. S. Speck, and Y.-R. Wu, "The influence of random indium alloy fluctuations in indium gallium nitride quantum wells on the device behavior," *Journal of Applied Physics*, vol. 116, no. 11, p. 113104, 2014.

[16] S. Marcinkevičius, R. Yapparov, L. Y. Kuritzky, Y.-R. Wu, S. Nakamura, and J. S. Speck, "Low-temperature carrier transport across InGaN multiple quantum wells: Evidence of ballistic hole transport," *Physical Review B*, vol. 101, p. 075305, Feb 2020.

[17] M. Luisier, A. Schenk, W. Fichtner, and G. Klimeck, "Atomistic simulation of nanowires in the $sp^3d^5s^*$ tight-binding formalism: From boundary conditions to strain calculations," *Physical Review B*, vol. 74, p. 205323, Nov 2006.

[18] S. Schulz, M. A. Caro, C. Coughlan, and E. P. O'Reilly, "Atomistic analysis of the impact of alloy and well-width fluctuations on the electronic and optical properties of InGaN/GaN quantum wells," *Physical Review B*, vol. 91, p. 035439, Jan 2015.

[19] M. Caro, S. Schulz, and E. OReilly, "Theory of local electric polarization and its relation to internal strain: Impact on polarization potential and electronic properties of group-III nitrides," *Physical Review B*, vol. 88, 09 2013.

[20] E. P. O. Reilly, A. Lindsay, S. Tomi, and M. Kamal-Saadi, "Tight-binding and k·p models for the electronic structure of Ga(In)NAs and related alloys," *Semiconductor Science and Technology*, vol. 17, pp. 870–879, Jul 2002.

[21] Z. Q. Li and W. Pötz, "Electronic density of states of semiconductor alloys from lattice-mismatched isovalent binary constituents," *Phys. Rev. B*, vol. 46, pp. 2109–2118, Jul 1992.

[22] T. B. Boykin, N. Kharche, G. Klimeck, and M. Korkusinski, "Approximate bandstructures of semiconductor alloys from tight-binding supercell calculations," *Journal of Physics: Condensed Matter*, vol. 19, p. 036203, Jan 2007.

[23] S. Birner, T. Zibold, T. Andlauer, T. Kubis, M. Sabathil, A. Trellakis, and P. Vogl, "nextnano: General Purpose 3-D Simulations," *IEEE Transactions on Electron Devices*, vol. 54, pp. 2137–2142, Sep. 2007.

[24] I. Vurgaftman and J. R. Meyer, "Band parameters for nitrogen-containing semiconductors," *Journal of Applied Physics*, vol. 94, no. 6, pp. 3675–3696, 2003.

[25] C.-Y. Tsai, C.-H. Chen, T.-L. Sung, C.-Y. Tsai, and J. M. Rorison, "Theoretical modeling of nonequilibrium optical phonons and electron energy relaxation in GaN," *Journal of Applied Physics*, vol. 85, no. 3, pp. 1475–1480, 1999.

[26] U. Özgr, X. Ni, X. Li, J. Lee, S. Liu, S. Okur, V. Avrutin, A. Matulionis, and H. Morkoç, "Ballistic transport in InGaN-based LEDs: Impact on efficiency," *Semiconductor Science and Technology*, vol. 26, p. 014022, 11 2010.

[27] Y. Huang, Z. Liu, X. Yi, Y. Guo, S. Wu, G. Yuan, J. Wang, G. Wang, and J. Li, "Overshoot effects of electron on efficiency droop in InGaN/GaN MQW light-emitting diodes," *AIP Advances*, vol. 6, no. 4, p. 045219, 2016.

[28] D. S. Sizov, R. Bhat, A. Zakharian, K. Song, D. E. Allen, S. Coleman, and C. Zah, "Carrier Transport in InGaN MQWs of Aquamarine- and Green-Laser Diodes," *IEEE Journal of Selected Topics in Quantum Electronics*, vol. 17, pp. 1390–1401, Sep. 2011.

[29] N. Kharch, M. Luisier, T. B. Boykin, and G. Klimeck, "Electronic structure and transmission characteristics of SiGe nanowires," *Journal of Computational Electronics*, vol. 7, pp. 350–354, 2008.

[30] T. B. Boykin, M. Luisier, A. Schenk, N. Kharche, and G. Klimeck, "The Electronic Structure and Transmission Characteristics of Disordered AlGaAs Nanowires," *IEEE Transactions on Nanotechnology*, vol. 6, no. 1, pp. 43–47, 2007.

[31] D. S. Tanner, P. Dawson, M. J. Kappers, R. A. Oliver, and S. Schulz, "Polar (In,Ga)N/GaN Quantum Wells: Revisiting the Impact of Carrier Localization on the "Green Gap" Problem," *Phys. Rev. Applied*, vol. 13, p. 044068, Apr 2020.

[32] T.-J. Y. Y.-R. Wu, C.K. Wu, "Influence of Random InGaN Alloy Fluctuations on GaN-Based Light-Emitting Diodes," in *Handbook of Optoelectronic Device Modelling and Simulation*

(J. Piprek, ed.), ch. 18, pp. 559–588, CRC Press, 2017.

[33] P. Dawson, S. Schulz, R. A. Oliver, M. J. Kappers, and C. J. Humphreys, "The nature of carrier localisation in polar and nonpolar InGaN/GaN quantum wells," *Journal of Applied Physics*, vol. 119, no. 18, p. 181505, 2016.

[34] C. M. Jones, C.-H. Teng, Q. Yan, P.-C. Ku, and E. Kioupakis, "Impact of carrier localization on recombination in InGaN quantum wells and the efficiency of nitride light-emitting diodes: Insights from theory and numerical simulations," *Applied Physics Letters*, vol. 111, no. 11, p. 113501, 2017.

[35] D. N. Nath, Z. C. Yang, C.-Y. Lee, P. S. Park, Y.-R. Wu, and S. Rajan, "Unipolar vertical transport in GaN/AlGaN/GaN heterostructures," *Applied Physics Letters*, vol. 103, no. 2, p. 022102, 2013.

[36] S. Marcinkevičius, R. Yapparov, L. Y. Kuritzky, Y.-R. Wu, S. Nakamura, S. P. DenBaars, and J. S. Speck, "Interwell carrier transport in InGaN/(In)GaN multiple quantum wells," *Applied Physics Letters*, vol. 114, no. 15, p. 151103, 2019.